

2-1-2012

Submicron Bioactive Glass Tubes for Bone Tissue Engineering

Jingwei Xie

Marshall University, xiej@marshall.edu

Eric Blough

Marshall University, blough@marshall.edu

Chi-Hwa Wang

Follow this and additional works at: http://mds.marshall.edu/miir_faculty

 Part of the [Medical Biotechnology Commons](#), and the [Musculoskeletal, Neural, and Ocular Physiology Commons](#)

Recommended Citation

Xie J, Blough ER, Wang CH. Submicron bioactive glass tubes for bone tissue engineering. *Acta Biomater.* 2012;8:811-819. (doi: 10.1016/j.actbio.2011.09.009)

This Article is brought to you for free and open access by the Marshall Institute for Interdisciplinary Research at Marshall Digital Scholar. It has been accepted for inclusion in Faculty Research by an authorized administrator of Marshall Digital Scholar. For more information, please contact zhangj@marshall.edu.

Submicron Bioactive Glass Tubes for Bone Tissue Engineering

Jingwei Xie^{a,b*}, Eric Blough^{b,c}, Chi-Hwa Wang^d

*^aMarshall Institute for Interdisciplinary Research, Marshall University, Huntington, WV, 25755
USA*

^bCenter for Diagnostic Nanosystems, Marshall University, Huntington, WV 25755, USA

^cDepartment of Biology, Marshall University, Huntington, WV 25755, USA

*^dDepartment of Chemical and Biomolecular Engineering, National University of Singapore,
Singapore, 4 Engineering Drive 4, 117576, Singapore*

*Corresponding Author

Jingwei Xie, Ph.D.

Marshall Institute for Interdisciplinary Research and Center for Diagnostic Nanosystems,
Marshall University

1700 Third Ave, Huntington, WV, 25755, USA

Phone: +1 (304) 696-3833

Fax: +1 (304) 696-3839

Email: xiej@marshall.edu

ABSTRACT

Herein we describe a method to fabricate submicron bioactive glass tubes using of sol-gel and co-axial electrospinning techniques for applications in bone tissue engineering. Heavy mineral oil and gel solution were delivered by two independent syringe pumps during the co-axial electrospinning process. Subsequently, submicron bioactive glass tubes were obtained by removal of poly(vinyl pyrrolidone) (PVP) and heavy mineral oil via calcination at 600 °C for 5 h. Tubular structure was confirmed by scanning electron microscopy (SEM) and transmission electron microscopy (TEM) imaging. We examined the bioactivity of submicron bioactive glass tubes and fibers and evaluated their biocompatibility taking electrospun poly(ϵ -caprolactone) fibers – a bio-inactive material for comparison. The bioactivity of glass tubes was examined in a simulated body fluid (SBF) and these structures demonstrated the formation of hydroxyapatite-like minerals on both the outer and inner surfaces. In contrast, mineralization only occurred on their surface for bioactive glass solid fibers. Energy dispersive x-ray (EDX) data suggested that bioactive glass tubes had a faster induction of mineral formation compared that observed for the solid fibers. We demonstrate that the proliferation rate of mouse pre-osteoblastic MC3T3-E1 cells on bioactive glass tubes was comparable to that on solid fibers. We also show that bioactive glass tubes can be loaded with a model protein drug - bovine serum albumin (BSA) and that these structures, exhibit delayed release properties. The bioactivity of released lysozyme can be as high as 90.9%. Taken together, these data suggest that submicron bioactive glass tubes could hold great potential for use in bone tissue engineering as well as topical drug or gene delivery.

Keywords: Bioactive glass, Electrospinning, Submicron Tubes, Bone tissue engineering, Drug delivery

1. Introduction

Bioactive glasses hold significant promise for hard tissue engineering as they are resorbable and readily form a bioactive hydroxycarbonate apatite (HCA) layer [1-3]. Bioactive glasses can also be tailored to deliver ions, i.e. Si, at levels capable of promoting cell differentiation and osteogenesis [4, 5]. Moreover, bioactive glasses also exhibit anti-inflammatory properties, anti-bacterial activity, and have been shown to stimulate the secretion of angiogenic growth factors *in vitro* [6-8]. Taken together, these properties suggest that these materials may be one of the most promising biomaterials for bone regeneration [9].

Bioactive glasses are generally formulated in the forms of bulk, crushed powders, foams, and micron-scale fibers. Owing to its high porosity and large surface area, a nonwoven mat of electrospun nanofibers can serve as an ideal scaffold to mimic the hierarchical architecture of extracellular matrix for cell attachment and nutrient transportation [10]. The nanofiber itself can also be functionalized through encapsulation and immobilization of bioactive materials such as extracellular matrix proteins, enzymes, and growth factors. In addition, the nanofibers can be further assembled into a variety of arrays or architectures by manipulating their alignment, stacking, or folding. Recently, bioactive glass nanofibers were developed using electrospinning and laser spinning techniques [11-14]. Although a significant advancement, it is likely that these nanofibers do not exhibit sufficient surface area for the rapid mineralization and enhancement of bone formation that can be critical for determining whether an implant will perform in an optimal fashion. To address this deficiency, recent work has attempted to fabricate hollow bioactive glass fibers via electrospinning where a high molecular weight poly(ethylene oxide) (PEO) is used as a phase-separation agent [15]. Whether these fibers are suited for bone tissue engineering applications has not been examined.

The objective of this study is to fabricate submicron hollow bioactive glass tubes and to examine the use of these structures in bone tissue engineering. Given the potential difficulties in accurately directing the formation of these types of structures using phase separation methods we chose to employ a sol-gel approach with the electrospinning process via the application of two syringe pumps to independently and precisely control the flow rates for the core and shell [16, 17]. Although similar approaches were reported for producing TiO₂ nanotubes, in the present study we demonstrated that a modified method can be used to generate submicron bioactive glass tubes with a more complicated composition than TiO₂ [16, 17]. And the inner and outer

diameters of tubes can be readily tailored by simply changing the feeding rates of inner and outer solutions during electrospinning process. This approach may be simpler and more robust than the phase separation method [15]. Compared to that observed for solid fibers, we hypothesized that the rate of HCA formation in a simulated body fluid (SBF) would be greater on the hollow fibers. The submicron bioactive glass tubes generated using this approach could be highly suited for use in bone tissue engineering applications.

2. Materials and methods

2.1. Fabrication of submicron bioactive glass tubes and fibers

A solution containing 1.34 g tetraethyl orthosilicate (TEOS) (Sigma-Aldrich, St. Louis, MO), 0.116 g triethyl phosphate (TEP) (Sigma-Aldrich), 0.296 g calcium nitrate ($\text{Ca}(\text{NO}_3)_2 \cdot 4\text{H}_2\text{O}$) (Sigma-Aldrich), 0.1 mL of HCL (Fisher, Pittsburgh, PA) solution (1 mol/L) and 10 mL ethanol (Fisher) was prepared. After stirring for 2 h, 10 mL of this solution was mixed with 10 mL of ethanol with 0.8 g poly(vinyl pyrrolidone) (PVP) (Sigma-Aldrich). Then, the mixed solution was stirred for another 2 h. Subsequently, the mixture was utilized for electrospinning with a coaxial spinneret, as outlined previously [17]. The typical feeding rate for PVP solution ranged from 1 to 2 mL/h. For the heavy mineral oil (Fisher), the feeding rate was set at 0.05 and 0.1 mL/h, respectively. The polymer PVP and heavy mineral oil were removed by sintering them at 600 °C for 5 h in air. For comparison, solid bioactive glass and poly(ϵ -caprolactone) (PCL) (Sigma-Aldrich) fibers were fabricated by traditional electrospinning as detailed previously [23, 24]. The bioactive glass tube sample for cell culture and drug delivery test was fabricated with injection rates of 1.5 mL/h and 0.05 mL/h for PVP solution and mineral oil, respectively. The corresponding fiber sample was fabricated with an injection rate of 1.5 ml/h for PVP solution.

2.2. Characterization of submicron bioactive glass tubes

Scanning electron microscopy (SEM) images and energy dispersive x-ray (EDX) spectroscopy were obtained by imaging the samples supported on a Si substrate with an FEI Sirion microscope at an accelerating voltage of 15 kV. Samples were sputtered with Au for 40 s before imaging. Transmission electron microscopy (TEM) images were obtained from samples supported on carbon-coated copper grids using a Philips CM100 TEM microscope with a Gatan 689 digital camera.

2.3. *In vitro* mineralization

The *in vitro* mineralization of submicron bioactive glass tubes and fibers was performed in a SBF for different time intervals. The composition of SBF consisted of 142 mM Na⁺, 5.0 mM K⁺, 1.5 mM Mg⁺, 2.5 mM Ca⁺, 147.8 mM Cl⁻, 4.2 mM HCO₃⁻, 1.0 mM HPO₄³⁻, and 1.0 mM SO₄²⁻ [25, 26]. At different time points, we quantified the Ca and Si ion concentrations in the SBF using inductively coupled plasma atomic emission spectroscopy (ICP-AES). Specifically, we firstly collected the solutions and then we diluted each solution by 5 times. ICP-AES was carried out using a Varian spectrometer Model Liberty 110.

2.4. *Cell culture and cell seeding*

Mouse calvaria-derived, preosteoblastic cells (MC3T3-E1; ATCC CRL-2593) were cultured in alpha minimum essential medium (α -MEM, Invitrogen Corp., Grand Island, NY), supplemented with 10% fetal bovine serum (FBS, Invitrogen), and 1% antibiotics (containing penicillin and streptomycin, Invitrogen). The medium was changed every other day, and the cultures were incubated at 37 °C in a humidified atmosphere containing 5% CO₂. Samples were cut into circular shape and fixed to the well edge of 96 well culture plates using medical grade silicone adhesive. Around 1×10⁴ cells were seeded to each well.

2.5. *Cell morphology observation*

The cell morphology at day 3 was characterized by fluorescent microscopy. The cells on the samples were washed twice with PBS, fixed in 3.7% formaldehyde solution (Sigma-Aldrich) in PBS for 30 min at room temperature, and dyed with Alexa Fluor® 488 phalloidin (Invitrogen) and 4'-6-Diamidino-2-phenylindole (DAPI, Invitrogen) for 1 h. The fluorescent images were taken using a QICAM Fast Cooled Mono 12-bit camera (Q Imaging, Burnaby, BC, Canada) attached to an Olympus microscope with Capture 2.90.1 (Olympus, Tokyo, Japan).

2.6. *Cell proliferation*

The cell viability was measured using the 3-(4, 5-dimethylthiazol-2, 5-diphenyl tetrazolium bromide (MTT) assay (Sigma-Aldrich), which is based on the mitochondrial conversion of tetrazolium salt. After 1, 3, 5 and 7 days of incubation, the medium was removed, 270 μ l fresh medium and 30 μ l MTT (5 mg/mL in PBS) (Invitrogen) were added to each well and incubated at 37 °C, 5% CO₂ for 3 h. After removal of the medium, the converted dye was dissolved with

isopropanol and the absorbance measured at 560 nm in triplicate using a microplate reader (Tecan, Durham, NC).

2.7. BSA loading and release

Submicron bioactive glass tube (10 mg) and fiber samples were immersed in 2 mL PBS buffer solution containing bovine serum albumin (BSA) (2 mg/mL) for 2 h. Samples were washed using water three times to remove any loosely attached molecules. BSA loading was determined by measuring the difference between the BSA concentration in the original solution and in the washes using a micro BCA protein assay kit. To determine the release kinetics, supernants were collected at several time intervals and the amount of BSA was measured as above.

2.8. Bioactivity of released biomacromolecules

Lysozyme was similarly loaded to the glass tubes. The bioactivity of the lysozyme released from tubes after 165-minute incubation was characterized by the rate of lysis of *Micrococcus lysodeikticus* cells by lysozyme [27]. Briefly, the experiments were carried out as follows. First, 2.5 mL of *Micrococcus lysodeikticus* cells in suspension was pipetted in 24 well plates. An aliquot of 0.1 mL of lysozyme solution at the same concentration of released and control samples (concentration determined by micro BCA assay kit) were added to the 24 well plates and tested by a microplate reader. The change in A_{450} per minute from the initial linear portion of the curve was recorded over 6 min. The bioactivity of lysozyme was deduced from the ratio of slopes of the two curves, namely, released lysozyme and native lysozyme.

2.8. Statistical analysis

All experiments were performed in triplicate, and data were presented as means \pm standard deviation, unless stated otherwise. Data were analyzed using one-way ANOVA with Tukey's HSD post hoc test to determine significance. Values of $P < 0.05$ were chosen to indicate statistical significance.

3. Results and discussion

3.1. Fabrication of submicron bioactive glass tubes and fibers

A schematic illustrating the preparation of submicron bioactive glass tubes is depicted in Fig. 1. A solution containing TEOS, TEP, $\text{Ca}(\text{NO}_3)_2 \cdot 4\text{H}_2\text{O}$, HCL, PVP and ethanol and heavy

mineral oil were introduced to the shell and core of a co-axial spinneret, respectively. After electrospinning, PVP and heavy mineral oil were removed by thermal treatment of the samples through converting them to CO₂ at 600 °C for 5 h. In addition, during the sintering process, TEOS, TEP and Ca(NO₃)₂ converted to SiO₂, P₂O₅ and CaO, respectively. For comparison, submicron bioactive glass and PCL fibers were generated using traditional electrospinning technique following our previous studies [23, 24]. Fig. 2A shows a representative SEM image of heavy mineral oil/PVP and glass composites core-sheath fibers as prepared after co-axial electrospinning. This sample was fabricated with injection rates for PVP solution and mineral oil of 1.5 mL/h and 0.05 mL/h, respectively. After sintering, tube diameter was decreased and cross sectional imaging indicated a tubular structure (Fig. 2B). The corresponding TEM images are shown in Figs. 2 C and D further confirming the shrinkage of diameter and the hollow structure. We also performed selective area electron diffraction (SAED) for submicron bioactive glass tubes and demonstrated an amorphous structure (Fig. S1A). EDX analysis suggested that the composition of bioactive glass tubes was 107SiO₂•69CaO•5P₂O₅. One advantage of this approach lies in the ease of controlling the inner and outer diameters by simply adjusting the inner and outer flow rates. After changing the inner and outer flow rates accordingly, the inner and outer diameters of tubes increased from 185 nm to 500 nm and 285 nm to 665 nm, respectively (Fig. S2).

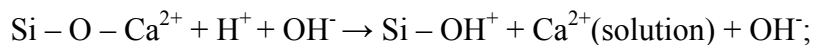
3.2. Bioactivity test

In order to test bioactivity, we immersed the glass tube samples in SBF at room temperature for different time intervals. For comparison, we also immersed the glass fiber samples in SBF under the same conditions. SEM images demonstrated that immersion in SBF for 1 day was found to result in HVA-like mineral clusters on the surface of the tubes (Fig. 3A) Inset in Fig. 3A shows a higher magnification image, presenting significant morphology change compared to the samples before immersion in SBF. Fig. 3B shows a TEM image of the same sample in Fig. 3A. As expected, we observed the presence of HCA-like minerals were not only on the outside but also inside the tubes. Similarly, prolonged immersion appeared to result in increased mineral deposition (Fig. 3C) on both the outside and inner surfaces (Fig. 3D). In addition, the results of selected area electron diffraction (SAED) analysis generated a pattern consistent with the presence of poorly crystallized apatite after 3 days of mineralization (Fig. S1B). In contrast to that observed for the tubes, imaging of the solid fibers indicated the presence of minerals on only

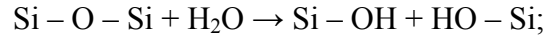
the outer surface (Fig. 3 E and F).

Elemental analysis on the bioactive glass tube and fiber samples after immersion in SBF over different periods of time was used to determine the atomic percentage of each element (Fig. 4A). Consistent with our imaging data, we observed that the percentage of Si and O atoms decreased with increasing immersion time. The percentages of Ca and P atoms showed opposite trends. Specifically, the percentage of Si atom for tubes dropped much faster than that observed using the solid fiber samples. The Si element was not detectable for tube samples after incubation for 3 days. In contrast, the percentage of Si element was around 7% for fiber samples under the same conditions. At the same time, the percentages of Ca and P atoms increased faster in the tube samples compared to that seen with the fibers. Taken together, these data demonstrate that the mineralization process is much faster on the tubes compared to that observed on the fibers as the reaction can occur not only outside but also inside tubes. Although not examined here, these data suggest that it is possible that bioactive glass tubes would form a biologically reactive hydroxycarbonate apatite layer in shorter period of time after implantation than solid fibers. We also used ICP-AES to quantify the ion concentrations in SBF after incubation with submicron glass tubes and fibers at different times (Fig. 4B). It shows that Ca and Si ion concentrations decrease and increase dramatically with increasing incubation time. Compared with fiber samples, more Ca ions were lost in the SBF solution after 3-day incubation with tube samples. Simultaneously, more Si ions were detected in the SBF incubated with tubes than with fibers for 3 days. In addition, Si ion concentration appeared to increase marginally from 2-day to 3-day incubation with glass tubes in the SBF, indicating that almost all the Si ions on glass tubes could move to the solution. This result seemed to agree well with that the EDX result – Si element was undetectable on glass tubes after 3-day incubation with SBF. The mechanism of mineralization for bioactive glass has been investigated by Hench [1]. We postulate that this mechanism is also suitable for explanation of the mineralization of bioactive glass tubes, and that it would involve the following steps:

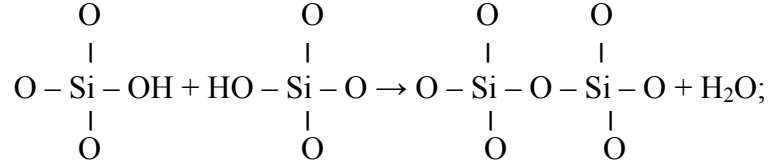
i) Rapid exchange of Ca^{2+} with H^+ or H_3O^+ from solution from both inner surface and outer surface of tubes:



ii) Loss of soluble silica in the form of $\text{Si}(\text{OH})_4$ to the solution, leading to breaking of Si-O-Si bonds and formation of Si-OH (silanols) at the inner and outer surfaces:



iii) Condensation and repolymerization of a SiO_2 -rich layer on the inner and outer surfaces depleted in alkalis and alkaline-earth cations:



iv) Migration of Ca^{2+} and PO_4^{3-} groups to the inner and outer surfaces through the SiO_2 -rich layer forming a $\text{CaO-P}_2\text{O}_5$ -rich film on top of the SiO_2 -rich layer, followed by growth of the amorphous $\text{CaO-P}_2\text{O}_5$ -rich film by incorporation of soluble calcium and phosphates from solution.

v) Crystallization of the amorphous $\text{CaO-P}_2\text{O}_5$ film by incorporation of OH^- and CO_3^{2-} anions from solution to form a mixed hydroxyl and carbonate apatite layer.

It is likely that immersion of the bioactive glass tubes into water can lead to the formation of minerals (Fig. 5). As prepared, the submicron tubes showed a smooth surface (Fig. 5A) however after immersion in water for 1 day, the surface became coarse (Fig. 5B) which may suggest that there is a rapid exchange of Ca^{2+} with H^+ or H_3O^+ from the solution which may be leading to the loss of soluble silica to the solution. After 3 days, the morphology had significantly changed (Fig. 5C) although the shape of tubes was still maintained. It seems that the tubes consisted of nanorods, which is a typical morphology of hydroxyl apatite. The length and width of nanorods were 100-200 nm and 5-10 nm, respectively. During this period of time, it is likely that the soluble silica was being continually being lost to the solution which may have helped in facilitating a reaction between Ca^{2+} and PO_4^{3-} to form hydroxyl apatite. After 6 days, the tubes were collapsed and only nanorods were observed under SEM (Fig. 5D). This finding is consistent with the possibility that prolonged incubation led to a breaking of all of the Si-O-Si bonds and the subsequent release of all soluble silica to the solution.

3.3. Cell culture

In order to test the potential of tubes for use as a bone scaffold, we cultured pre-osteoblastic MC3T3-E1 cells on the submicron bioactive glass tubes. We chose electrospun PCL fibers for comparison because PCL is a biocompatible and biodegradable but bio-inactive material and has been used for bone tissue engineering [28]. After 3 days of culture, cells were stained with Alexa Fluor® 488 phalloidin (green) to visualize F-actin, while cell nuclei were stained with DAPI (blue). We observed that although the cells can spread very well on the surface of PCL fibers, the cell density was lower compared to other two samples based on the counting of nuclei (Fig. 6A-C). It appeared that more cell nuclei were observed on the bioactive glass tube sample and that these cells exhibited a high level of actin organization as most of the stress fibers appeared to be orientated in a parallel fashion (Fig. 6C). By utilization of MTT assay, we attempted to quantify the MC3T3-E1 cell proliferation (Fig. 7) [29]. Here, we assume all the cells have the same level of metabolic activity on different substrates. While there was no difference between the samples at day 1, after 3 days of culture the OD values for cells on the bioactive glass tubes were significantly higher than those of PCL fibers ($P < 0.05$). The MTT assay is measuring metabolic activity, which is proportional to cell number in normal conditions. However, the cells were compared on different substrates in the present work and the cells were likely to have a different metabolic activity on the different substrates (e.g., cells may be more active on the glass tubes.). Therefore, it is possible that this assay an indirect measurement could not accurately measure cell number. The use of a direct measurement of cell number (e.g., DNA assay and pico green) to quantify the cell number on each substrate will be more appropriate for further study.

3.4. BSA loading and release

For bone tissue engineering, the incorporation of growth factors (e.g., bone morphogenic proteins) to bone scaffolds and the sustained release of these proteins from scaffolds is highly desirable for the effective regeneration of bone [30, 31]. To examine the potential utility of bioactive glass tubes for this type of application these structures were loaded with BSA and we then determined the release kinetics. BSA was chosen as a model protein drug as it has been previously used for these types of experiments [32, 33]. For purposes of comparison, parallel experiments were carried out using submicron bioactive glass fibers. Drug loading and release were quantified by micro BCA protein assay kit. The amount of BSA that could be loaded into

the submicron bioactive glass tubes and fibers was 82.98 $\mu\text{g}/\text{mg}$ and 66.63 $\mu\text{g}/\text{mg}$, respectively. Fluorescence microscopy after incubation with FITC-BSA appeared to demonstrate a uniform distribution of FITC-BSA into the bioactive glass tubes (Fig. 8A-B). Analysis of the release kinetics demonstrated an initial burst of BSA liberation into the solution followed by a certain period of delayed release (Fig. 8C). After incubation for 165 min, no BSA was detected from the fiber samples, whereas BSA release was still detectable from the tube samples (Fig. 8D). This finding is consistent with the possibility that drug release occurs over a longer duration in the tube samples. This could be due to the morphology change of tubes after incubation in the releasing medium.

3.5. Bioactivity of released biomacromolecules

In order to test the bioactivity of biomacromolecules after release, we prepared lysozyme-loaded, submicron bioactive glass tubes. The concentration of released lysozyme from glass tubes after 165-minute incubation was quantified by the Micro BCA assay kit. The same concentration of fresh lysozyme solution was prepared. The bioactivity was characterized by the rate of lysis of *M. lysodeikticus* cells. The bioactivity of lysozyme during the loading and releasing process was around 90.9%, which can be deduced from the ratio of the slopes from the two lines shown in Fig. 9 [32].

4. Conclusions

We have demonstrated the fabrication of submicron bioactive glass tubes by injecting heavy mineral oil and gel solution to the core and shell independently during co-axial electrospinning followed by sintering to remove polymer and heavy mineral oil. This approach is simple, versatile and robust. *In vitro* bioactivity test indicates bioactive glass tubes had a faster induction of HCA-like mineral formation compared to solid fibers. Pre-osteoblastic cells showed a higher proliferation rate on submicron bioactive glass tubes than on PCL fibers. In addition, the model protein drug BSA showed a longer period of release from bioactive glass tubes than that observed using the solid fibers. The bioactivity of released lysozyme from glass tubes can be as high as 90.9%. This novel class of bioactive glass could be promising for applications in bone tissue engineering and drug delivery.

Acknowledgements

This study was supported by start-up funds from Marshall Institute for Interdisciplinary Research (MIIR) and Center for Diagnostic Nanosystems (CDN) at Marshall University. The authors would like to thankfully acknowledge Prof. Aley El-Shazly and Miss Kelli Elizabeth Gagnon from Department of Geology at Marshall University for generously assisting with ICP-AES measurement.

References

- [1] Hench LL. Bioceramics. *J Am Ceram Soc* 1998; 81: 1705-1728.
- [2] Hench LL. The story of bioglass®. *J Mater Sci Mater Med* 2006; 17: 967-978.
- [3] Bunting S, Silvio LD, Deb S, Hall S. Bioresorbable glass fibers facilitate peripheral nerve regeneration. *J Hand Surg* 2005; 30B: 242-247.
- [4] Xynos D, Edgar AJ, Buttery LDK, Hench LL, Polak JM. Gene-expression profiling of human osteoblasts following treatment with the ionic products of Bioglass® 45S5 dissolution. *J Biomed Mater Res* 2001; 55: 151-157.
- [5] Jell G, Stevens MM. Gene activation by bioactive glasses. *J Mater Sci Mater Med* 2006; 17: 997-1002.
- [6] Lepparanta O, Vaahtio M, Peltola T, Zhang D, Hupa L, Hupa M, Ylanen H, Jukka IS, Matti KV, Eerola E. Antibacterial effect of bioactive glasses on clinically important anaerobic bacteria in vitro. *J Mater Sci Mater Med* 2008; 19: 547-551.
- [7] Eberhard J, Reimers N, Dommisch H, Hacker J, Freitag S, Acil Y, Albers HK, Jepsen S. The effect of the topical administration of bioactive glass on inflammatory markers of human experimental gingivitis, *Biomaterials* 2005; 26: 1545-1551.
- [8] Day RM. Bioactive glass stimulates the secretion of angiogenic growth factors and angiogenesis in vitro. *Tissue Eng* 2005; 11: 768-777.
- [9] Hench LL, Polak JM. Third-generation of biomedical materials. *Science* 2002; 295: 1014-1017.
- [10] Xie J, Li X, Xia Y. Putting electrospun nanofibers to work for biomedical research. *Macromol Rapid Commun* 2008; 29: 1775-1792.
- [11] Kim HW, Kim HE, Knowles JC. Production and potential of bioactive glass nanofibers as a next-generation biomaterial. *Adv Funct Mater* 2006; 16: 1529-1535.
- [12] Xia W, Zhang D, Chang J. Fabrication and in vitro biomineralization of bioactive glass (BG) nanofibers. *Nanotechnology* 2007; 18: 135601.
- [13] Hong Y, Chen X, Jing X, Fan H, Guo B, Gu Z, Zhang X. Preparation, bioactivity, and drug release of hierarchical nanoporous bioactive glass ultrathin fibers. *Adv Mater* 2010; 22: 754-758.

- [14] Quintero F, Pou J, Comesana R, Lusquinos F, Riveiro A, Mann AB, Hill RG, Wu ZY, Jones JR. Laser spinning of bioactive glass nanofibers. *Adv Funct Mater* 2009; 19: 3084-3090.
- [15] Hong Y, Chen X, Jing X, Fan H, Gu Z, Zhang X. Fabrication and drug delivery of ultrathin mesoporous bioactive glass hollow fibers. *Adv Funct Mater* 2010; 20: 1503-1510.
- [16] Li D, Xia Y. Fabrication of titania nanofibers by electrospinning. *Nano Lett* 2003; 3: 555-560.
- [17] Li D, Xia Y. Direct fabrication of composite and ceramic hollow nanofibers by electrospinning. *Nano Lett* 2004; 4: 933-938.
- [18] Li D, McCann JT, Xia Y. Use of electrospinning to directly fabricate hollow nanofibers with functionalized inner and outer surfaces. *Small* 2005; 1: 83-86.
- [19] Kim JW, Song JH, Kim HE. Bioactive glass nanofiber-collagen nanocomposite as a novel bone regeneration matrix. *J Biomed Mater Res* 2006; 79A: 698-705.
- [20] Kim HW, Lee HH, Chun GS. Bioactivity and osteoblast responses of novel biomechanical nanocomposites of bioactive glass nanofiber filled poly(lactic acid). *J Biomed Mater Res* 2008; 85A: 651-663.
- [21] Lee HH, Yu HS, Jang JH, Kim HW. Bioactivity improvement of poly(ϵ -caprolactone) membrane with the addition of nanofibrous bioactive glass, *Acta Biomater* 2008; 4: 622-629.
- [22] Noh KT, Lee HY, Shin US, Kim HW. Composite nanofibers of bioactive glass nanofiller incorporated poly(lactic acid) for bone regeneration. *Mater Lett* 2010; 64: 802-805.
- [23] Xie J, Willerth SM, Li X, MacEwan MR, Rader A, Sakiyama-Elbert SE, Xia Y. The differentiation of embryonic stem cells seeded on electrospun nanofibers into neural lineages. *Biomaterials* 2009; 30: 354-362.
- [24] Xie J, Wang CH. Electrospun micro- and nanofibers for sustained delivery of paclitaxel to treat C6 glioma in vitro. *Pharm Res* 2006; 23: 1817-1826.
- [25] Li X, Xie J, Yuan X, Xia Y. Coating electrospun poly(ϵ -caprolactone) fibers with gelatin and calcium phosphate and their use as biomimetic scaffolds for bone tissue engineering. *Langmuir* 2008; 24: 14145-14150.
- [26] Nandakumar A, Yang L, Habibovic P, Blitterswijk C. Calcium phosphate coated electrospun fiber matrices as scaffolds for bone tissue engineering. *Langmuir* 2009; 26: 7380-7387.

- [27] Ghaderi R, Carlfors. Biological activity of lysozyme after entrapment in poly (d,l-lactide-co-glycolide) microspheres. *Pharm Res* 1997; 14: 1556-1562.
- [28] Yoshimoto H, Shin YM, Vacanti JP. A biodegradable nanofiber scaffold by electrospinning and its potential for bone tissue engineering. *Biomaterials* 2003; 24: 2077-2082.
- [29] Taira M, Nakao H, Takahashi J, Araki Y. Effects of two vitamins, two growth factors and dexamethasone on the proliferation of rat bone marrow stromal cells and osteoblastic MC3T3-E1 cells. *J Oral Rehabilitation* 2003; 30: 697-701.
- [30] Nie H, Soh BW, Fu YC, Wang CH. Three-dimensional fibrous PLGA/Hap composite scaffold for BMP-2 delivery. *Biotech & Bioeng* 2008; 99: 223-234.
- [31] Fu YC, Nie H, Ho ML, Wang CK, Wang CH. Optimized bone regeneration based on sustained release from three-dimensional fibrous PLGA/Hap composite scaffolds loaded with BMP-2. *Biotech & Bioeng* 2008; 99: 996-1006.
- [32] Xie J, Wang CH. Encapsulation of proteins in biodegradable polymeric microparticles using electrospray in the Taylor cone-jet mode. *Biotech & Bioeng* 2007; 97: 1278-1290.
- [33] Xie J, Ng WJ, Lee LY, Wang CH. Encapsulation of protein drugs in biodegradable microparticles by co-axial electrospray. *J. Colloid Interface Sci* 2008; 317: 469-476.

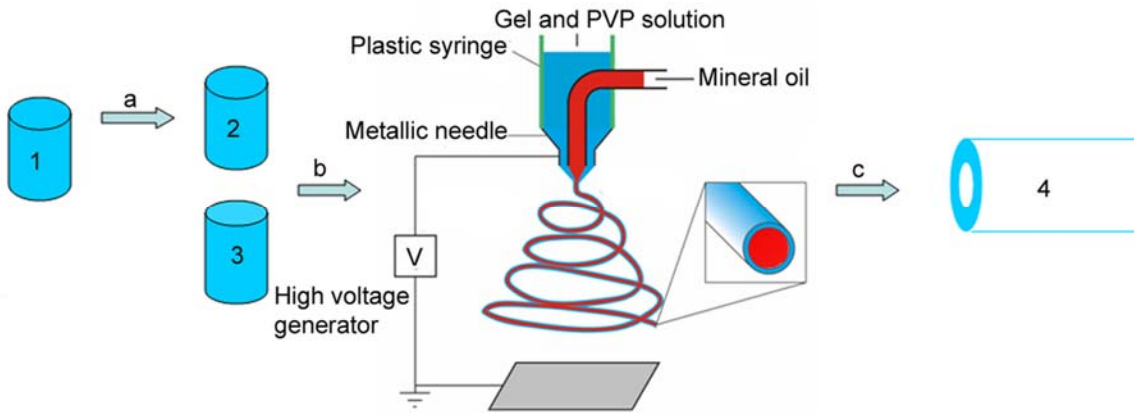


Fig. 1. Schematic illustrating preparation of submicron bioactive glass tubes. (a): Aging the sol solution for 2 h. (b) Mixing gel solution and PVP solution for 2 h. (c) Sintering at 600 °C for 5 h. (1) Sol solution (TEOS, TEP, $\text{Ca}(\text{NO}_3)_2 \cdot 4\text{H}_2\text{O}$, HCl, Ethanol). (2) Gel solution. (3) PVP ethanol solution. (4) Bioactive glass tubes.

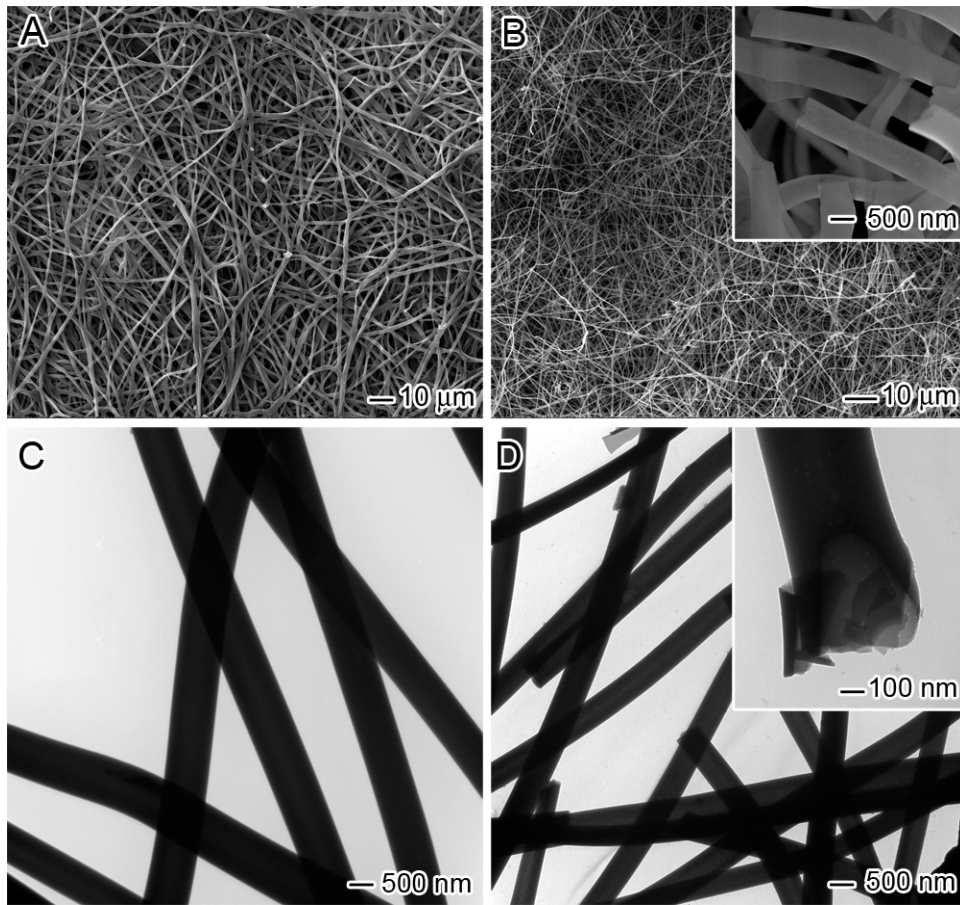


Fig. 2. (A) SEM image of submicron PVP/glass composite tubes before sintering. (B) SEM image of submicron bioactive glass tubes after sintering. (C) TEM image of submicron PVP/glass composite tubes before sintering. (D) TEM image of submicron bioactive glass tubes after sintering. Insets: higher magnification images. This sample was fabricated with injection rates of 1.5 mL/h and 0.05 mL/h for PVP solution and mineral oil, respectively.

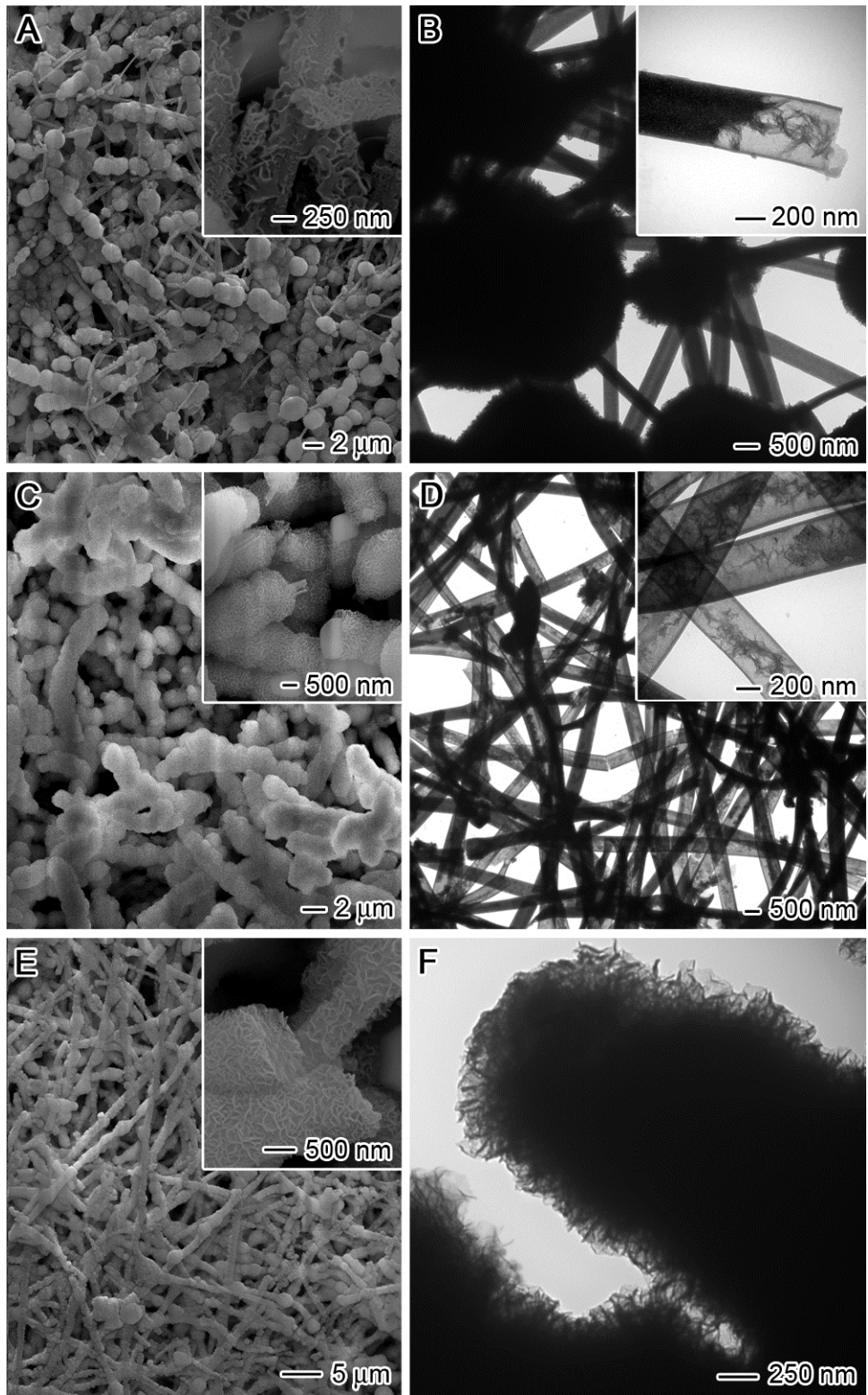


Fig. 3. SEM images of submicron bioactive glass tubes after immersion in SBF for 1 day (A) and 3 days (C). TEM images of submicron bioactive glass tubes after immersion in SBF for 1 day

(B) and 3 days (D). Particles detected in (C) but not in (D) could be due to washing during TEM sample preparation. (E) SEM image of submicron bioactive glass solid fibers after immersion in SBF for 3 days. (F) TEM image of bioactive glass solid fibers after immersion in SBF for 3 days. The tube sample was fabricated with injection rates of 1.5 mL/h and 0.05 mL/h for PVP solution and mineral oil, respectively. The fiber sample was fabricated with an injection rate of 1.5 mL/h for PVP solution.

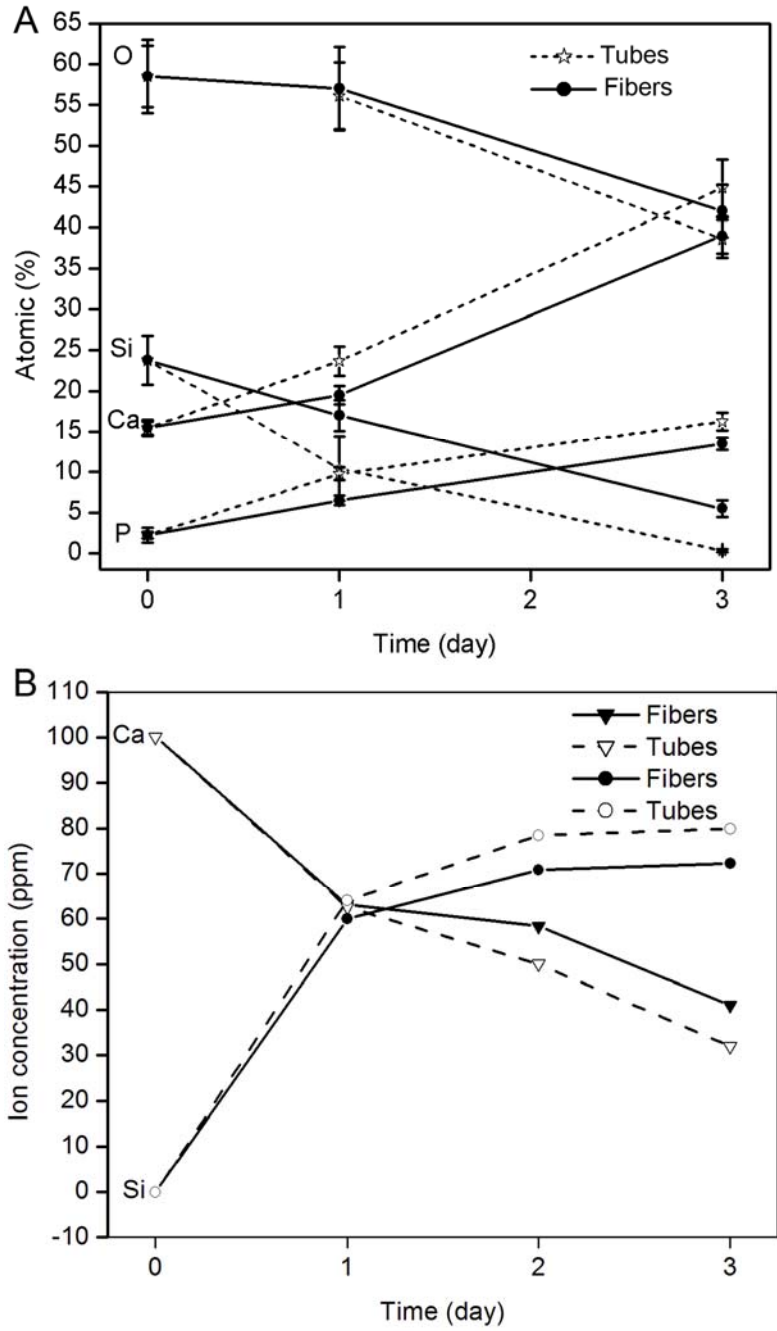


Fig. 4. (A) Elemental analysis via EDX of submicron bioactive glass tubes and fibers after immersion in SBF over different periods of time. (B) Ion concentrations in SBF were quantified by ICP-AES after incubation with submicron bioactive glass tubes and fibers at different times.

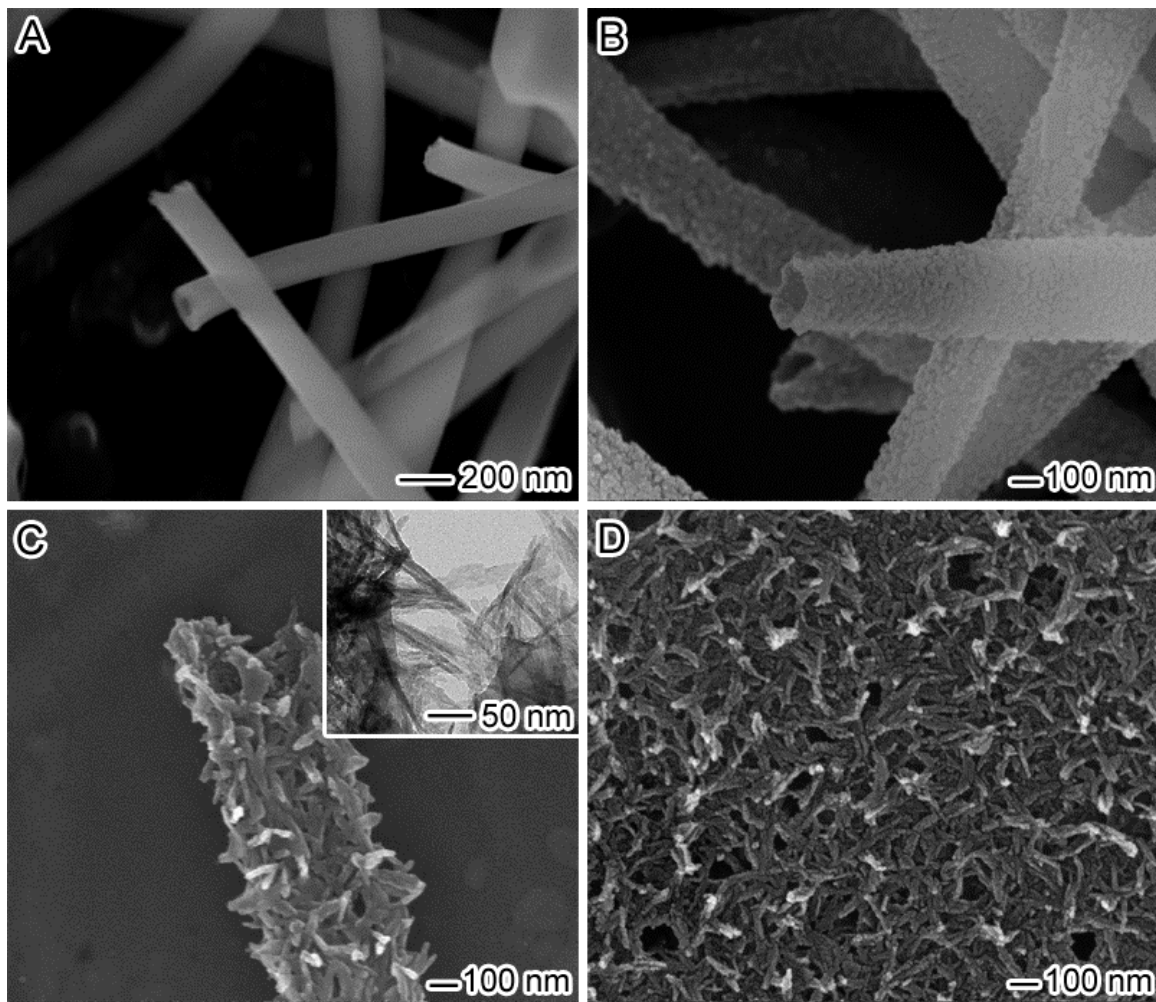


Fig. 5. SEM images of submicron bioactive glass tubes (A), after immersion in water for 1 day (B); 3 days (C); and 6 days (D). Inset: TEM image showing the surface of tubes. This sample was fabricated with injection rates of 1.0 mL/h and 0.05 mL/h for PVP solution and mineral oil, respectively.

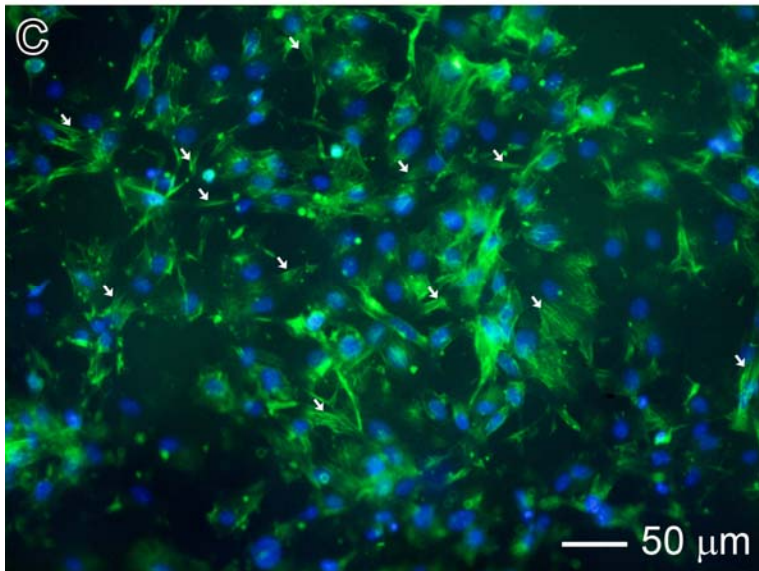
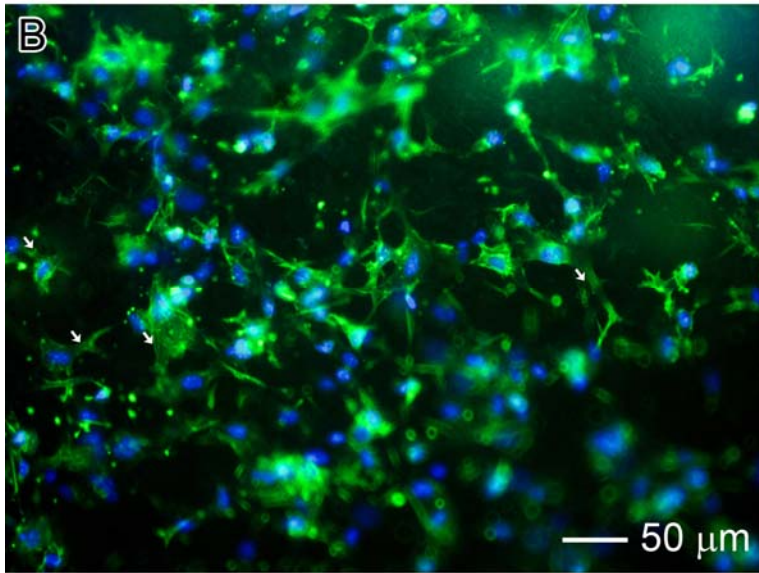
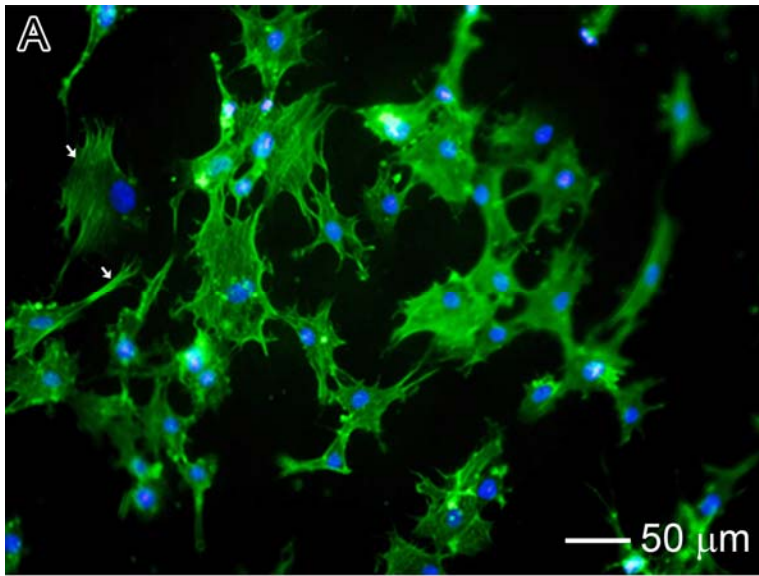


Fig. 6. Representative fluorescence microscopy images showing MC3T3-E1 cell morphology after culturing for 3 days on electrospun PCL fibers (A), bioactive glass fibers (B), and bioactive glass tubes (C). The F-actin of cells was stained with Alexa Fluor® 488 phalloidin (green), while the cell nucleus was stained with 4'-6-Diamidino-2-phenylindole (DAPI) (blue). White arrows indicate stress fibers and actin organizations.

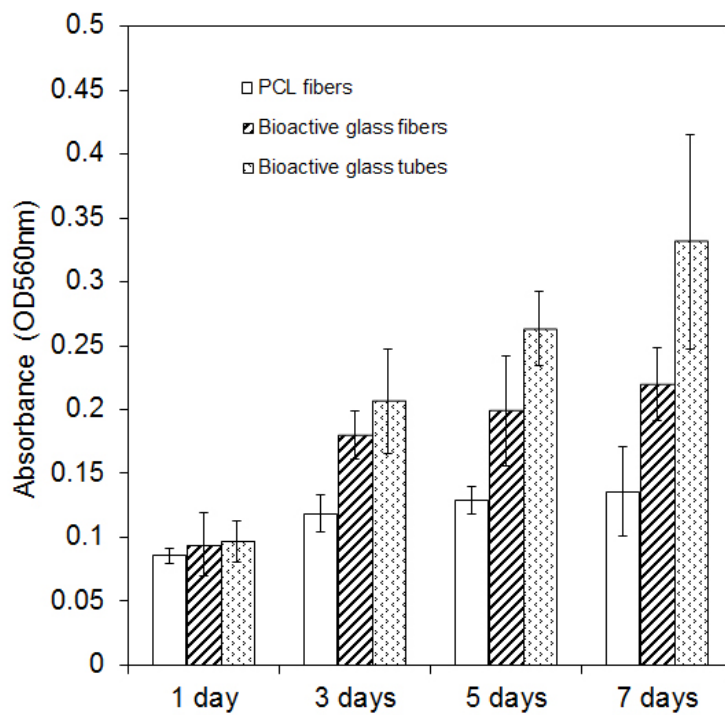


Fig. 7. Cell proliferation on different substrates quantified by MTT assay.

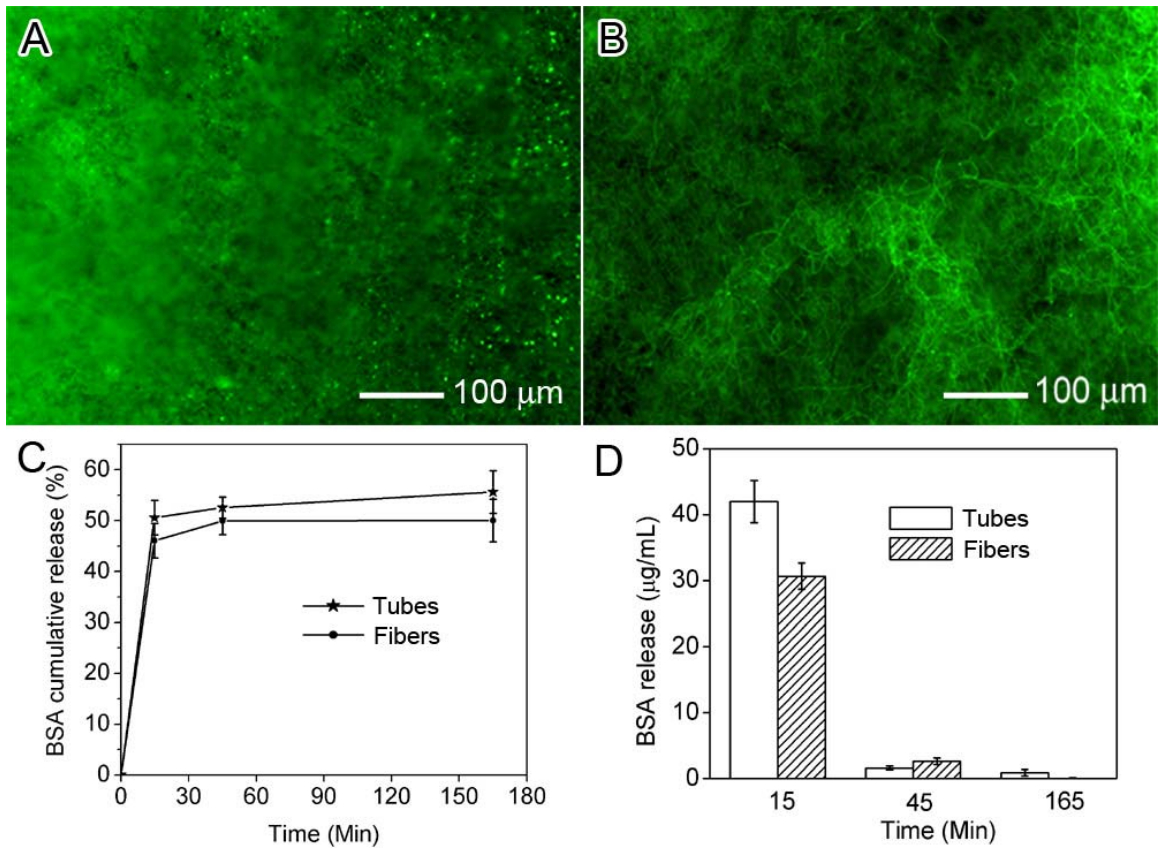


Fig. 8. Fluorescence micrographs showing submicron bioactive glass fibers (A) and tubes (B) after adsorption of FITC-BSA. (C, D) *In vitro* release of BSA from submicron bioactive glass tubes and fibers.

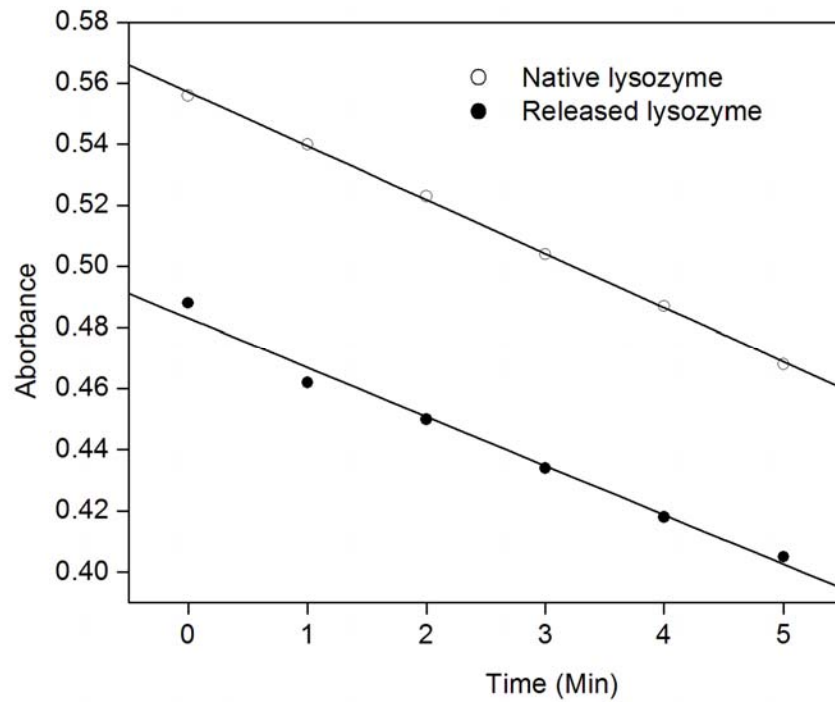


Figure 9. Lysozyme bioactivity test (y: absorbance; x: time). ○: linear fit of released lysozyme after incubation for 165 minutes, $y = -0.0161x + 0.483$, $R^2 = 0.9876$; ●: linear fit of native lysozyme, $y = -0.0177x + 0.5571$, $R^2 = 0.9993$.

Bioactive Glass Nanotubes for Bone Tissue Engineering

Jingwei Xie^{a,b*}, Eric Blough^{b,c}, Chi-Hwa Wang^d

*^aMarshall Institute for Interdisciplinary Research, Marshall University, Huntington, WV, 25755
USA*

^bCenter for Diagnostic Nanosystems, Marshall University, Huntington, WV 25755, USA

^cDepartment of Biology, Marshall University, Huntington, WV 25755, USA

*^dDepartment of Chemical and Biomolecular Engineering, National University of Singapore,
Singapore, 4 Engineering Drive 4, 117576, Singapore*

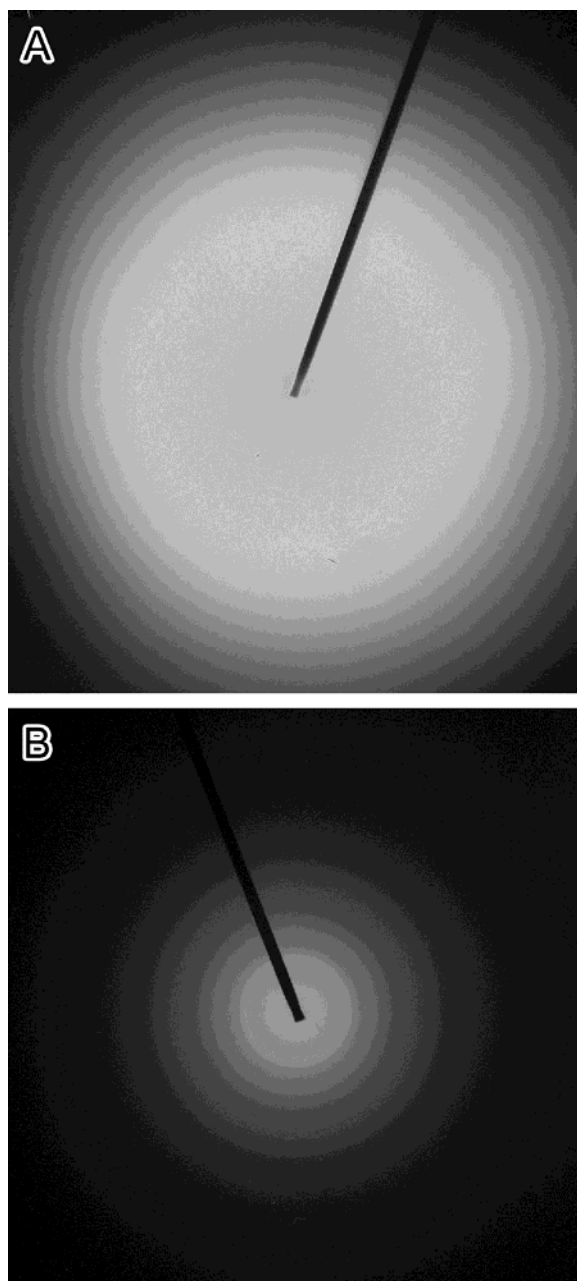


Fig. S1. SAED pattern of bioactive glass nanotubes before (A) and after immersion in SBF for 3 days (B).

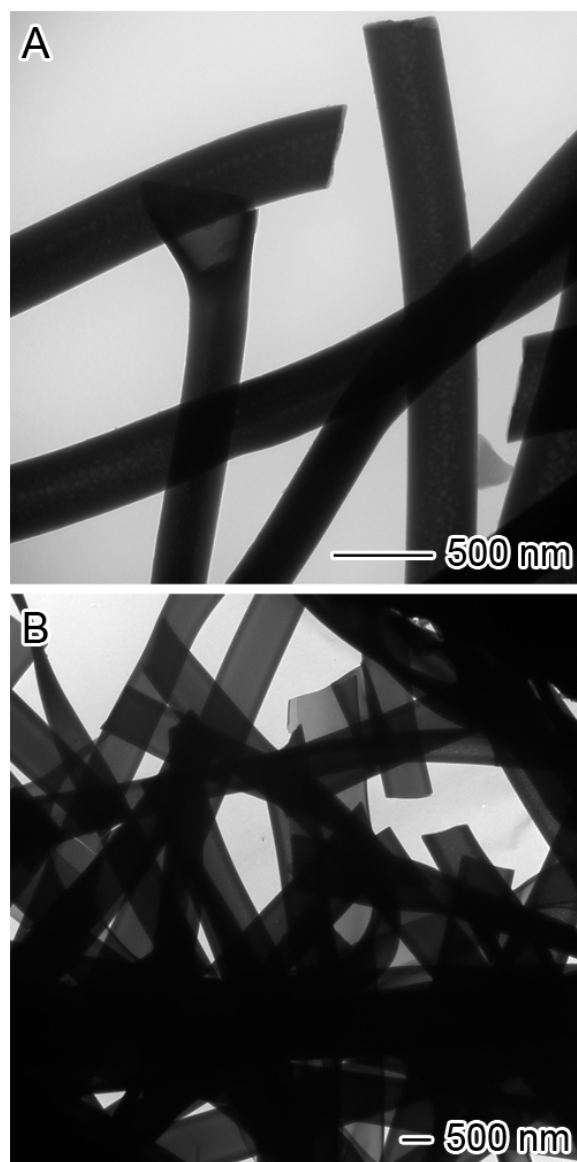


Fig. S2. TEM images of bioactive glass nanotubes. (A) The sample was fabricated with injection rates of 1 mL/h and 0.05 mL/h for PVP solution and mineral oil, respectively. (B) The sample was fabricated with injection rates of 2 mL/h and 0.1 mL/h for PVP solution and mineral oil, respectively.